Vibrational Spectroscopy of Peptides and Peptide−Water Complexes: Anharmonic Coupled-Mode Calculations

S. K. Gregurick, E. Fredj, R. Elber, and R. B. Gerber*

Department of Physical Chemistry and the Fritz Haber Center for Molecular Dynamics, The Hebrew University of Jerusalem, Jerusalem 91904, Israel, and The Department of Physical Chemistry, University of California, Irvine, California, 92711

Received: May 14, 1997; In Final Form: August 13, 1997[⊗]

Quantum calculations are reported for vibrational states and energy levels of several peptide and peptide−water complexes, to provide insight into the spectroscopic properties of such systems and their dependency on presently available anharmonic force fields. A blocked di-L-serine−H_2O complex and trialanine in an antiparallel β sheet configuration are the main systems treated. The calculations are for variants of the Amber force field and use the vibrational self-consistent field (VSCF) method, which includes effects of anharmonicity as well as interactions between modes. The main findings are as follows: (1) Distinct isomers of a single peptide−H_2O complex corresponding to different hydrogen binding sites of the H_2O are observed. (2). The H_2O induces shifts of up to 50 cm^{-1} in the frequencies of fundamental transitions associated with the peptide modes. (3). Some of the "intermolecular" modes of the peptide−H_2O cluster are of frequencies and geometry that suggest effective peptide-to-water energy transfer. (5). Changing the TIP3 water potential in the Amber force field into the Coker−Watts potential produces significant spectroscopic changes. (5). The peptide−H_2O cluster is found to have several tunneling states, which are assigned in detail. At least some of these states should be spectroscopically observable by the magnitude of the splitting. (6) The trialanine calculations are compared with experimental data available for part of the transitions. For many of the "stiff" transitions good agreement is found, but the remaining differences suggest that the force field should be revised. It is argued on the basis of these results that high-resolution spectroscopy in jets should be an excellent tool for improving and developing biomolecular force fields.

I. Introduction

The understanding of the structure and dynamics of biological molecules, e.g. proteins, requires a reliable, physically realistic representation of the molecular force field. Present day force fields for proteins are based mostly on thermodynamic and X-ray data, on ab initio calculations, and to a lesser extent on spectroscopy of small organic molecules. For a detailed description of force fields for biological molecules, see for example McCammon and Harvey,[1] Cornell et al.,[2] Jorgensen et al.,[3] and Brooks et al.[4] For small or intermediate size molecules, high-resolution spectroscopy has been primarily the main tool for the development of highly accurate potential functions,[5−9] and it is expected to benefit the optimization of force fields for biomolecules as well. There may thus be merit in combining spectroscopic techniques such as high-resolution IR,[10−15] Raman,[16,17] inelastic neutron scattering[18,19] and electronic absorption spectroscopy data[20,21] with quantum mechanical calculations of spectroscopic frequencies and intensities. There have indeed been steps in this direction, attempting to refine potentials by fitting spectroscopic data, e.g. for hydrocarbons[22,23] and proteins.[24,25] However for proteins, the task is quite demanding in part because the solvent interferes with the spectrum, causing a broadening and a shift of the frequencies. Furthermore, the relatively high temperatures in which the spectrum is obtained make isolation of one or a few minima virtually impossible. There are also theoretical challenges to predicting vibrational spectra, one of which is to include the anharmonic and mode-coupling effects. Previously, this was possible only for relatively small systems, with only a few degrees of freedom.[26−30]

The possibility of high-resolution molecular spectroscopy enables a more global fit of the potential energy surface. However, any such fit of spectroscopy must be based on a theory which also allows for the quantum mechanical, anharmonic mode-coupled nature of proteins. There is evidence that the VSCF method is quite reliable for a fully quantum calculation which implicitly includes these effects.[29,31] Furthermore, Roitberg et al. illustrated that such a calculation is feasible for relatively large systems.[32] The aim of the present work is to expand on these original calculations in order to both gain insight into the physical properties of hydrogen-bonded complexes and test typical force fields. The two systems we have studied, di-L-serine and trialanine, will offer a unique test of the current force field, as will be illustrated below. Our current approach is quite novel, in that it is the first such calculation to rigorously test the all-atom force field of Cornell and coworkers.[2]

Previous calculations of the vibrational states of biological molecules relied mostly on a harmonic approximation (HA), which inherently neglects both the anharmonicity and mode-coupling effects (for examples see ref 11 and references therein). It is also possible to calculate the vibrational states of biomolecules using classical trajectories, but these calculations would inherently neglect the quantum effects.[33] One could improve slightly on the HA method by either a quasi-harmonic approximation[34,35] or a higher order Taylor series expansion.[32,36] Utilizing a VSCF method, we have investigated the solvation effects of a small peptide−water system. Furthermore, we have looked into the role the force field plays in the vibrational spectrum. We also investigate the possible identification of different conformers based solely on the vibrational spectrum,

[⊗] Abstract published in *Advance ACS Abstracts,* October 1, 1997.

S1089-5647(97)01587-3 CCC: $14.00

and last we have investigated some purely quantum behavior of the peptide−water system, namely tunneling effects.

The paper is organized as follows: Section I is dedicated to the description of the potential energy surface of proteins in general, while section II is a description of the VSCF method. The results and discussion sections are IV and V. Section V of the results focuses on di-L-serine, and section V deals with the larger system trialanine in antiparallel β sheet configuration. Within section IV are the effects due to solvation, the validity of the full VSCF calculation, and the tunneling states of the system. Our paper ends with the conclusions in section VI.

II. Potential Energy Surface

In our VSCF calculations, we utilized an all-atom force field as implemented in the molecular dynamics program MOIL.[37] This force field is widely used in protein dynamics, and hence our calculations will serve as a benchmark test for the potential. The functional form for the potential takes the standard from and is as follows:[2]

$$V(\vec{R}) = \sum_{\text{bonds}} K_r(r - r_{\text{eq}})^2 + \sum_{\text{angles}} K_\theta(\theta - \theta_{\text{eq}})^2 + \sum_{\text{dihedrals}} \frac{V_n}{2}[1 + \cos(n\phi - \gamma)] + \sum_{i<j}\left[\frac{A_{ij}}{R_{ij}^{12}} - \frac{B_{ij}}{R_{ij}^{6}} + \frac{q_i q_j}{\epsilon R_{ij}}\right] + \sum_{i<j}\left[\upsilon_{14}\left(\frac{A_{ij}}{R_{ij}^{12}} - \frac{B_{ij}}{R_{ij}^{6}}\right) + \text{el}_{14}\frac{q_i q_j}{\epsilon R_{ij}}\right] \quad (2.1)$$

Here $\vec{R}$ is a vector containing the *x,y,z* coordinates of all the atoms, *r* represents the norm of the bonding vector between any two connected atoms, and θ is the angle between any three bonded atoms. The dihedral angle, ϕ, includes both proper and improper torsions, where γ is a phase factor and V_n is the torsional barrier parameter. The last two terms in eq 2.1 represent the van der Waals and electrostatic interactions, which is calculated between atoms either of different molecules or on the same molecule but separated by at least three bonds ($\upsilon_{14} = 8$ and $\text{el}_{14} = 1.2$). Here R_{ij} is the distance between atoms *i* and *j*, A_{ij}, $B_{i,j}$ are the van der Waals parameters, and q_i is the partial charge on atom *i*. Cornell and co-workers found it necessary to set the electrostatic scaling factor, ϵ, to 1 in order to reproduce the interaction energies of the small molecules used as a basis for the potential. All molecular parameters for the implementation of this force field can be found in ref 2.

We utilized two different force fields to describe the solvent inter- and intramolecular interactions. The first model was the standard rigid TIP3 OPLS (optimized potential for liquid simulations), developed by Jorgensen.[3] The form of the TIP3 OPLS potential is exactly the same as in the protein (eq 2.1), and there are no additional terms to describe hydrogen bonding. The TIP3 OPLS potential places emphasis on reproducing experimental densities and heats of vaporization for liquids. For the stability of the SHAKE algorithm as implemented in MOIL the bond and angle force constants were chosen such that the resulting intramolecular water force field is relatively rigid. The second model we utilized was a flexible four-point model developed by Coker and Watts.[38] In this potential, the water intramolecular force field is described as a Morse function in local modes. The intermolecular water−water potential is the semiempirical RWK2 model of Reimers and co-workers.[39] This potential includes both an atom−atom Coulombic interaction and a dispersion interaction which is exponentially damped. There is an additional Coulombic term describing the attraction between the H atom on one molecule and the negative charge located at the bisector of the HOH angle on the second molecule. The solvent−protein interaction is described exactly the same as in the TIP3 model, except that the water−oxygen charge no longer resides on the oxygen atom. Using this potential, the calculated vibrational frequencies for the water dimer were found to be in quite good agreement with the experimental frequencies.[38] Subsection B in the Results and Discussion section will focus on how changes in the solvent force field can drastically alter the resulting spectrum.

III. VSCF Method

In general, the solution to the *N*-dimensional Schrödinger equation for the vibrational states of the protein can be quite difficult to solve. In normal mode coordinates this equation has the following form:

$$\left[-\frac{\hbar^2}{2}\sum_{j=1}^{N}\frac{\partial^2}{\partial Q_j^2} + V(Q_1,...,Q_N)\right]\Psi(Q_1,...,Q_N) = E\Psi(Q_1,...,Q_N) \quad (3.1)$$

where Q_j is the mass-weighted normal mode coordinate, *V* is the full potential which includes anharmonicity and coupling between all of the modes, and *N* is the number of degrees of freedom ($3 \times N_{\text{atoms}} - 6$) in the protein. One may simplify eq 3.1 by utilizing the separable Hartree approximation, which is the basis of the VSCF method:[26−28,40]

$$\Psi(\vec{Q}) = \prod_{k=1}^{N}\psi_k(Q_k) \quad (3.2)$$

This then leads to *N* single mode VSCF equations of the following form:

$$\left[-\frac{\hbar^2}{2}\frac{\partial^2}{\partial Q_k^2} + V_{\text{VSCF}}(Q_k) - \epsilon_k\right]\psi_k(Q_k) = 0 \quad (3.3)$$

where the effective potential for mode *k* is given by

$$V_{\text{VSCF}}(Q_k) = \langle\prod_{l\neq k}^{N}\psi_l(Q_l)|V(Q_1,...,Q_N)|\prod_{l\neq k}^{N}\psi_l(Q_l)\rangle \quad (3.4)$$

Equations 3.3 and 3.4 for the single mode wave functions, energies, and effective potentials must be solved self-consistently. We can, however, make use of the following fact: in the vicinity of a local/global minimum the total potential energy of the system can be approximated as a Taylor series expansion in normal modes. The harmonic approximation (HA) takes advantage of this by expanding only up to the quadratic term, where Q_k is defined as the displacement from equilibrium:

$$V_{\text{HA}}(\vec{Q}) = \sum_{k=1}^{N}\left[V_k(Q_{\text{eq}}) + \frac{\partial V}{\partial Q_k}(Q_k - Q_{\text{eq}}) + \frac{1}{2}\frac{\partial^2 V}{\partial Q_k^2}(Q_k - Q_{\text{eq}})^2\right] \quad (3.5)$$

The main simplicity of this approximation stems from the fact that the modes become completely separable. This is also the main disadvantage, because although the calculation of the energy is simplified, valuable information, e.g. the anharmonic and mode-coupling effects, has been disregarded. These effects can be included by continuing the expansion as follows (note

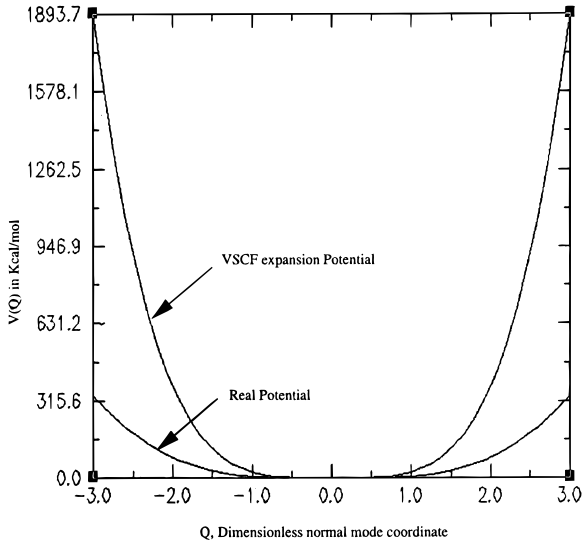

Figure 1. Comparison between the quartic expansion of the methyl rotational mode and the true potential for this mode.

$Q_k = (Q_k - Q_{eq})$, and as we are at a minimum the first-order term vanishes):

$$V(\vec{Q}) = \frac{1}{2}\sum_{k=1}^{N}\frac{\partial^2 V}{\partial {Q_k}^2}{Q_k}^2 + \frac{1}{6}\sum_{k=1}^{N}\frac{\partial^3 V}{\partial {Q_k}^3}{Q_k}^3 + \frac{1}{24}\sum_{k=1}^{N}\frac{\partial^4 V}{\partial {Q_k}^4}{Q_k}^4 + \frac{1}{2}\sum_{k=1}^{N}\sum_{l\neq k}^{N}\frac{\partial^3 V}{\partial {Q_k}^2 Q_l}{Q_k}^2 Q_l + \frac{1}{4}\sum_{k=1}^{N}\sum_{l\neq k}^{N}\frac{\partial^4 V}{\partial {Q_k}^2 {Q_l}^2}{Q_k}^2 {Q_l}^2 + \ldots \quad (3.6)$$

In eq 3.6, the diagonal terms represent anharmonic effects, while the off-diagonal terms are the coupling between different modes. We have neglected the cubic and higher order terms with nonrepeating indices ($Q_kQ_lQ_m$, $Q_kQ_lQ_mQ_n$), as they will be exceedingly small and in fact vanish in a perturbation treatment which uses the harmonic approximation as the unperturbed Hamiltonian.[41] For $n > 2$ the expansion coefficients, $\partial^n V/\partial {Q_k}^n$, were calculated using finite differences.[42] The quartic expansion (eq 3.6) suffices for such systems, if one studies low-lying vibrational states, as was illustrated by Jung and Gerber for small H_2O clusters. Jung and Gerber found that the inclusion of MP2 (Möller−Plesset perturbation theory) corrections to the quartic expansion were quite small, particularity as the water cluster size increased.[31] Since we are interested in fundamental transitions only, the quartic expansion will be valid for many modes. However, some systems do exhibit strong anharmonic effects, as illustrated in the $(H_2O)_n$ clusters.[31] We have also found evidence for such strong anharmonic effects for the methyl rotational modes which occur near 300 cm^{-1}. For these modes, the true potential (Figure 1) is nearly a boxlike potential, as also seen in low-frequency modes of the water clusters.

Equation 3.6 is valid for expansion about a single minimum. In principle, the spectroscopy depends on the specific isomeric structure, and in previous studies different minima showed different spectroscopic frequencies. This may actually become a source of important information in the future, when experiments can be performed in which molecules are prepared in different conformations. Thus for a complete spectroscopic study of all conformations, a separate expansion for each unique conformer will be required.

In our system, the normal modes are near-separable as the off-diagonal mode-coupling terms will most likely not dominate the expansion. In this case the total wave function may still be written as a product over the single-mode wave functions. Because the potential is nonseparable, the Hamiltonian is likewise nonseparable, or not exactly solvable. However, by making use of the Hartree approximation (eq 3.2), the problem can be solved in an iterative fashion. Within this approximation the coupled potential $V(\vec{Q})$ is reduced to N effective single-mode potentials, which are averaged over all the other modes in the following manner:

$$V_{VSCF}(Q_k) = \frac{1}{2}\frac{\partial^2 V}{\partial {Q_k}^2}{Q_k}^2 + \frac{1}{6}\frac{\partial^3 V}{\partial {Q_k}^3}{Q_k}^3 + \frac{1}{24}\frac{\partial^4 V}{\partial {Q_k}^4}{Q_k}^4 + \frac{1}{2}\sum_{l\neq k}^{N}\frac{\partial^3 V}{\partial {Q_k}^2 Q_l}{Q_k}^2 \langle\psi_l(Q_l)|Q_l|\psi_l(Q_l)\rangle + \frac{1}{4}\sum_{l\neq k}^{N}\frac{\partial^4 V}{\partial {Q_k}^2 {Q_l}^2}{Q_k}^2 \langle\psi_l(Q_l)|{Q_l}^2|\psi_l(Q_l)\rangle \quad (3.7)$$

The VSCF expression for the total energy of vibrational state n is thus a sum of all the individual mode energies minus a term that accounts for the double counting of the modes and has the following form:

$$E^n_{total} = \sum_{k=1}^{N}\epsilon_k^n - (N-1)\langle\prod_{k=1}^{N}\psi_k^n|V(Q_1,\ldots,Q_N)|\prod_{k=1}^{N}\psi_k^n\rangle \quad (3.8)$$

In our present calculation, we solved each k VSCF Hamiltonian (eq 3.3) using the collocation method of Yang and Peet.[43] For an adjustable grid, sensitive to each mode, we choose to work in the dimensionless variable, $\bar{q}_k$, where

$$\bar{q}_k = \frac{Q_k}{(\lambda_k)^{1/4}} \quad (3.9)$$

Here λ_k is the kth eigenvalue of the Hessian. Convergence was determined when $\Delta\sum_k\epsilon_k \leq 0.0001$ kcal/mol from one iteration to the next. The initial calculations were carried out on a Silicon Graphics Indigo workstation, and later the VSCF program was parallelized with an MPI interface on an IBM-SP2 cluster architecture.

IV. Results and Discussion: Di-L-serine

A. Structure and Energetics. We began with the neutral methyl-blocked peptide, di-L-serine. This system was chosen as a reasonably typical nonionic small peptide structure. A good candidate for a low-energy minimum was found by the method of local enhanced sampling (LES).[44,45] The number of LES copies was set to 10. These copies were annealed for 5 ps at a rate of 0.5 fs with the initial temperature at 300 K and the final temperature at 10 K. The resulting structures were further minimized by a steepest descent method. From the resulting minimized LES copies, the lowest energy structure is shown in Figure 2. To this low-energy conformer, one H_2O molecule was annealed to different possible hydrogen-binding sites on the peptide. From the many possible local minima, we choose four conformers to study the effects of solvation. The four local minima are shown in Figure 3, and Table 1 lists their energetic properties. We can see from Figure 3 and Table 1 that conformer 1 is the lowest energy structure (−89.57 kcal/mol), while conformer 3 is the highest (−84.62 kcal/mol). Conformer 1 has three peptide−water hydrogen bonds and is expected to exhibit a rigid H_2O−peptide spectrum. In contrast, the other

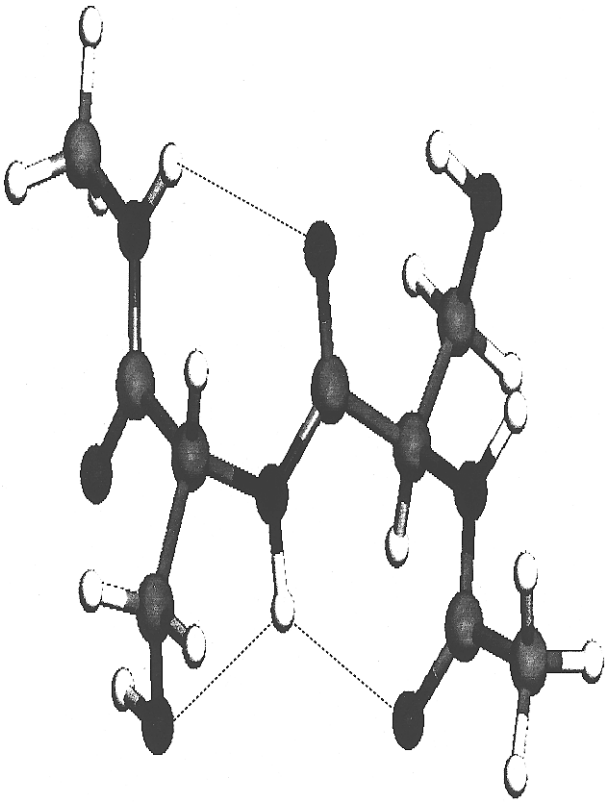

Figure 2. Lowest energy structure of di-L-serine, found by the LES method. The dotted lines illustrate intramolecular hydrogen bonding.

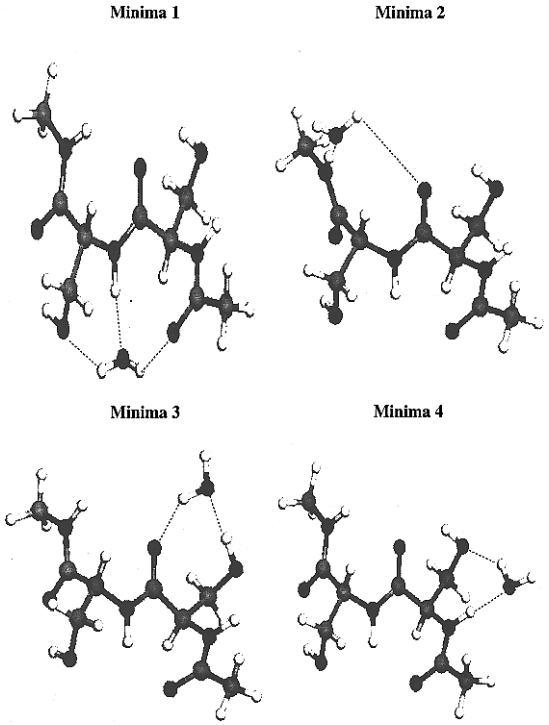

Figure 3. Four different conformers of the di-L-serine−H_2O complex. The dotted lines illustrate intermolecular hydrogen bonding.

conformers have on average two peptide−water hydrogen bonds. Conformer 3 offers a unique test of hydrogen bonding through the hydroxyl residue of the serine amino acid. This conformer has the weakest hydrogen bonds and will exhibit the most floppy H_2O−peptide spectrum. We also give the ϕ and ψ angles for the backbone torsions.

B. Effect of the H_2O Intramolecular Force Field. One of the goals of our investigation is to determine how sensitive

TABLE 1: Di-L-serine−H_2O Complex (All Energies in kcal/mol)

energetics	conformer 1	conformer 2	conformer 3	conformer 4
total energy	−89.563	−85.047	−84.620	−86.079
bond energy	0.396	0.355	0.694	0.477
angle energy	1.615	1.626	3.044	1.339
torsion energy	0.910	1.433	3.316	0.680
improper torsions	0.053	0.037	0.036	0.042
van der Waals	0.572	−1.849	1.270	0.971
electrostatic	−156.0	−151.6	−157.2	−151.4
1−4 electrostatic	59.128	60.870	60.349	58.004
1−4 van der Waals	3.569	4.058	3.790	3.681
(ϕ, ψ) angle *N*-end	(75, −100)	(77, −93)	(80, −74)	(78, −83)
(ϕ, ψ) angle C-end	(82, −82)	(69, −131))	(72, −109)	(73, −94)

TABLE 2: Table of Di-L-serine−H_2O Spectrum (All Frequencies Are in cm^{-1})[a]

CW	TIP3	difference	assignment
3863.081	3896.949	−33.868	H_2O(aS)
3619.893	3848.435	228.542	H_2O(sS)
1752.879	2865.513	−1112.633	H_2O(b)
1718.823	1750.353	−31.530	amide I
1688.339	1717.452	−29.112	amide I
705.311	767.061	−61.750	concerted hydrogen motion
525.620	519.581	6.039	NH(b), CN(t) coupled to H_2O
552.865	589.907	−37.043	CC(S), CN(t) coupled to H_2O
416.916	428.009	−11.093	CCN(t), NH(b), CO(S)···H_2O
191.107	196.404	−5.297	CH_3 rotation (CC(t))
266.465	262.118	4.346	CH_3 rotation (CC(t))
45.579	56.207	−10.628	delocalized backbone motion
43.359	40.081	3.278	delocalized backbone motion

[a] aS = asymmeteric stretch, sS = symmetric stretch, b = bend, and t = torsion.

the vibrational spectrum is to changes in the force field. The current standard TIP3 water potential is rigid. In MOIL, the bond and angle "stretching" force constants were adjusted such that the SHAKE dynamics were stable, rather than reproducing physical properties. This will lead to some vibrational frequencies in the MOIL model that are higher than expected. To make a comparison between the two different force fields, we have calculated the vibrational SCF spectrum for both the TIP3 and the Coker−Watts (CW) peptide−H_2O system (for conformer 1). Table 2 lists some of the frequencies and the difference between the frequencies, which is also shown in Figures 4 and 5. We see immediately that while most frequencies are nearly identical for the two force fields, several frequencies differ by an appreciable amount. Most notable is the water bending frequency (2865 vs 1752 cm^{-1}), which was expected. However, other frequencies are also effected by the coupling between the peptide−solvent force field, (the H_2O stretching modes at 3800, the amide I mode at 1750, and the modes of concerted hydrogen motion at 760, 600, and 430 cm^{-1}). The difference spectrum illustrates that there is significant coupling between the solvent and some of the protein degrees of freedom. This coupling may lead to possible energy transfer between the protein and solvent modes. In Figure 6 we illustrate the coupling between one peptide amide I mode and the H_2O bending mode, which is expected to show strong energy transfer as these two frequencies are near-resonant (1752 and 1718 cm^{-1}).[46] We conclude that the intramolecular H_2O potential is significantly affecting the spectroscopic properties. Furthermore, these results suggest that high-resolution spectroscopic measurements will be quite useful in improving the H_2O−protein potential. Hereafter, all of our calculations will use the Coker−Watts water potential.

C. Harmonic Approximation vs the Full SCF Calculation. We have also investigated the importance of the full quartic expansion (eq 3.7) compared to the harmonic approximation

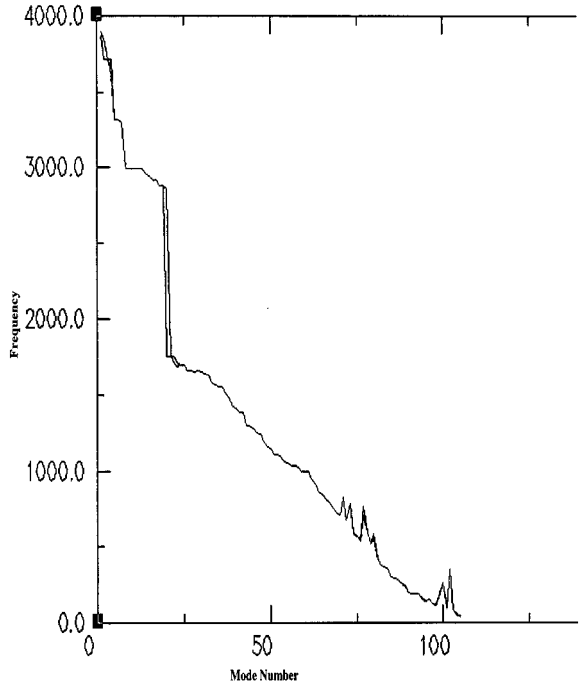

Figure 4. VSCF vibrational energies calculated using the TIP3 and CW force field. The mode number is the numerical enumeration of the modes (from highest (3863 cm^{-1}) to lowest (43 cm^{-1}) frequency).

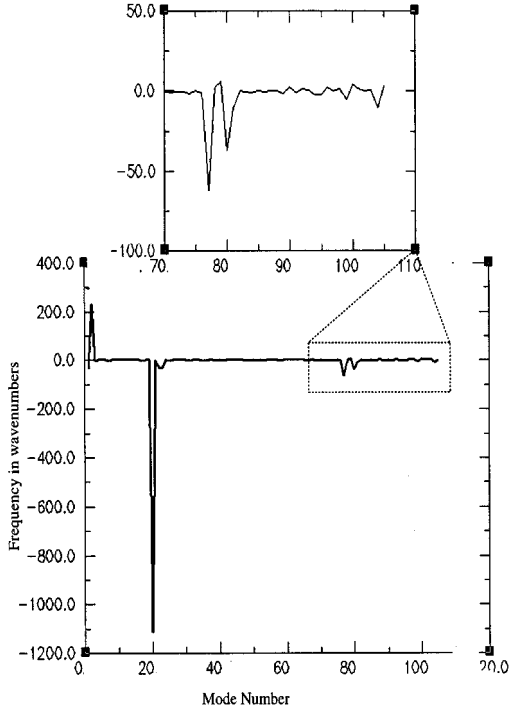

Figure 5. Difference spectrum between the SCF vibrational energies calculated using the TIP3 and CW force field. The mode number is the numerical enumeration of the modes (from highest (3863 cm^{-1}) to lowest (43 cm^{-1}) frequency).

(eq 3.5). Figure 7 illustrates the difference spectrum between the full and the harmonic SCF vibrational frequencies. It is quite clear that most of the modes are blue shifted from the corresponding harmonic values. This is due to the anharmonic and mode coupling terms, which act in such a way as to stiffen the effective potential of each mode. In other words, our peptide$-H_2O$ system is more rigid than the harmonic approximation would predict. Two modes, the H_2O symmetric stretch and one of the serine amide I modes, are red-shifted. The red/blue shift of the H_2O asymmetric/symmetric stretch

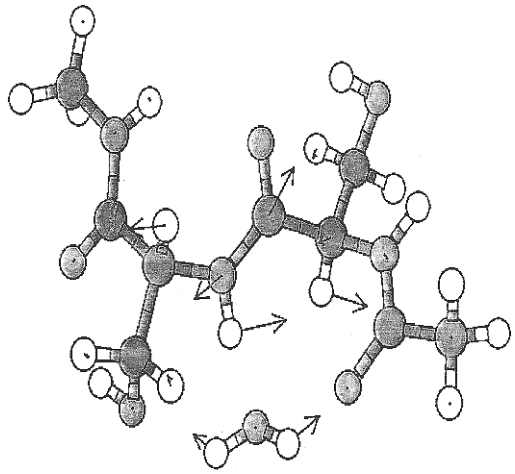

Figure 6. Mode 22: The coupling between one of the peptide amide I modes and the H_2O bending mode.

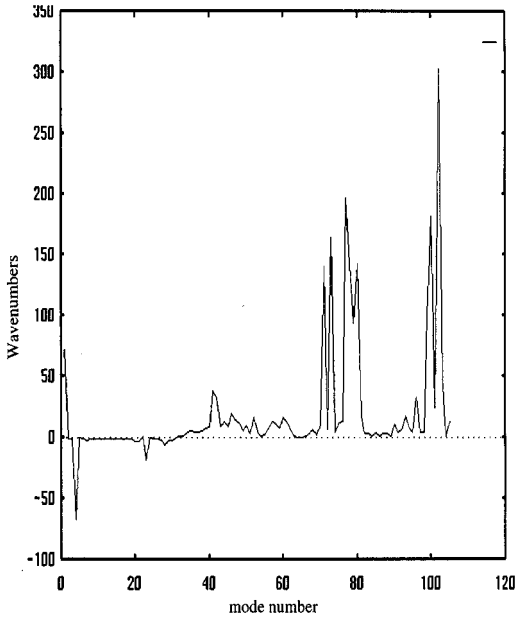

Figure 7. Difference spectrum between the full SCF vibrational frequencies and the harmonic frequencies.

indicates that the description of hydrogen bonding is rather anharmonic, and thus the harmonic frequencies deviate rather strongly from their VSCF counterparts. In previous work of small H_2O clusters, Jung and Gerber noticed a pronounced blue shift indicative of larger anharmonic and mode-coupling effects.[29] The four modes which are blue shifted by 100 cm^{-1} (modes 75−81) are torsional modes of the peptide$-H_2O$ system, and the two highly blue shifted (300 cm^{-1}) modes (modes 100 and 102) are those that correspond to the methyl rotation. As stated earlier (Figure 1), these modes are very anharmonic and were treated in a DVR type of approach. In the DVR approach, the modes associated with the methyl rotation were represented on a grid of points, rather than the expansion of eq 3.7. The coupling between the modes was however the same as in the expansion method.

D. Spectroscopically Distinguishing between Isomers. One of the main goals of our present investigation was to be able to spectroscopically distinguish between different conformers of the same minimum structure. Table 3 is a comprehensive list of all of the main characteristic modes and the frequencies of each of the corresponding conformers. The modes were assigned by an analysis of the corresponding eigenvectors from the diagonalization of the Hessian matrix. We find that, in

TABLE 3: Table of Characteristic Frequencies (in cm^{-1})[a]

mode	conformer 1	conformer 2	conformer 3	conformer 4
H_2O (aS)	3863	3955.9	3792.4	3816.2
(sS)	3619.9	3708.4	3685.7	3642.7
(b)	1752.8	1751.9	1750.6	1753.2
L-Ser OH(S)	3715.2	3715.4	3712.1	3713.4
	3715.2	3714.1	3685.6	3713.5
NH(S)	3319.9	3320.7	3321.1	3319.1
	3313.8	3319.7	3317.1	3317.5
	3300.5	3289.6	3314.2	3293.0
CH(S)	2993.5	2993.9	2993.9	2994.4
	2993.5	2993.7	2993.5	2993.6
	2992.9	2993.4	2993.4	2993.1
	2992.7	2993.3	2993.1	2993.4
	2993.1	2993.3	2992.7	2992.9
	2960.6	2956.6	2947.9	2948.4
	2920.6	2920.9	2921.1	2921.5
	2920.7	2920.6	2920.7	2920.9
	2878.8	2878.6	2878.9	2878.7
	2876.8	2876.9	2876.9	2877.3
CH_3(ab)	1657.4	1658.2	1658.1	1657.6
	1654.2	1654.9	1654.2	1657.6
	1651.7	1653.0	1654.1	1655.8
	1651.2	1652.0	1651.0	1654.8
CH_3(sb)	1477.2	1479.4	1481.7	1481.4
	1425.1	1429.2	1469.4	1444.6
band	conformer 1	conformer 2	conformer 3	conformer 4
amide I	1718.8	1717.4	1709.8	1711.6
	1699.6	1701.3	1701.4	1701.8
	1696.0	1694.5	1694.5	1700.9
	1688.4	1654.9	1647.5	1673.
	1661.6	1662.3	1664.4	1666.
	1642.8	1637.2	1638.4	1641.
	1629.1	1625.4	1631.9	1630.
amide II	1585.9	1582.5	1582.9	1587.7
	1565.1	1558.2	1559.3	1571.9
	1558.3	1553.6	1549.7	1563.0
	1551.8	1546.8	1544.6	1555.0
amide III	1410.3	1390.3	1383.2	1401.6
	1302.9	1295.4	1297.2	1308.0
	1301.2	1293.1	1293.7	1300.9
	1247.9	1260.4	1267.7	1293.9
	1249.5	1254.4	1244.1	1273.7
	1241.1	1245.7	1229.8	1241.5
	1195.2	1205.7	1184.9	1186.2
	1164.5	1164.9	1162.8	1171.7
	1150.5	1141.9	1149.1	1159.6
	1107.3	1108.9	1102.1	1105.1
	1110.9	1103.5	1103.4	1104.7
	1089.4	1087.0	1084.2	1113.3
alcohol(D)	1387.4	1367.7	1423.8	1388.4
	1379.8	1364.1	1393.3	1388.6
alcohol CO(aS)	1057.2	1055.4	1057.7	1059.2
	1053.9	1051.5	1053.7	1056.4
new H_2O modes	199.7	180.9	172.7	194.9
	192.2	171.2	123.4	177.1
	187.7	160.8	86.4	151.1
	139.8	94.8	66.7	135.1
	152.3	77.8	35.9	213.3
	111.7	45.4	0.5	75.3

[a] aS = asymmetric stretch, sS = symmetric stretch, b = bend, and t = torsion.

addition to each of the separate H_2O and peptide modes, there are *six* new modes which correspond to motion of the H_2O in the planes of the peptide. These new modes are highly characteristic of the hydrogen-bonding environment of the H_2O. For example, we see that for conformer 1 these six frequencies are relatively high in comparison to the other conformers. This may be explained by the fact that this conformer has three hydrogen bonds, whereas the others have on average two. However, for conformer 3 we see just the opposite. This conformer illustrates a relatively weakly hydrogen bonded conformer, particularly for motion along the peptide backbone from the N to C terminus (0.5 cm^{-1}). This frequency may be in error, as it is within the resolution of our potential, however there should be a very low lying excitation for this mode. These distinctive frequencies may serve as a spectroscopic tag for various hydrogen-bonding environments. In many of the other characteristic modes (e.g. NH stretch, H_2O bend, CH stretch, alcohol asymmetric stretch, and CH_3 asymmetric−symmetric bends) the frequencies are quite similar between conformers, which illustrates that overall the conformers do have a similar peptide backbone structure. However a few of the modes provide a clear distinction between different conformers. In particular, in conformer 3, which is the only conformer with the hydroxyl as the donor hydrogen for the hydrogen bond, we see very distinctive behavior in the H_2O symmetric stretch (3650 cm^{-1}) and OH deformation (1420 cm^{-1}) modes. These frequencies are quite characteristic for hydrogen-bonded systems where the alcohol is the hydrogen donor.[47,48] Another interesting feature of our spectra is the frequency shifts in the amide I mode, which also exhibits energy-transfer possibilities (Figure 6). The amide I mode corresponds to a CO and CN stretch and CO bend along the peptide backbone and is characteristic of the protein secondary structure. In conformer 1, which has direct coupling between the peptide and the H_2O bend, the frequency is blue shifted by 50 cm^{-1}. The amide II modes (NH in-plane bend) are quite similar between each conformer, and in the amide III modes (NH in-plane bend + CN stretch) the conformer frequencies can differ by up to 20 cm^{-1}. This mode is quite difficult to characterize, as it is sensitive to the backbone and side chain conformation. We also see from Table 3 that the CH_3 asymmetric bending mode is a bit too high (by 200 cm^{-1}) compared to the experimental IR frequency (1440 cm^{-1}). In an attempt to determine the effect of additional water molecules on the fundamental frequencies, we added one H_2O molecule from a randomly chosen position. The new structure was annealed with the same simulated annealing schedule as before, and the VSCF frequencies were calculated for the resulting structure. With additional waters around the peptide structure, the CH_3 asymmetric bending mode does fall within the experimental value (Figure 8). However, only this mode showed such a strong shift in frequency, as all the other modes remained near their original values. The experimental frequency range for the CO alcohol asymmetric stretch is 1075−1000 cm^{-1}, in agreement with our calculated values of 1050 cm^{-1}. The alcohol deformation is 1420 cm^{-1} if hydrogen bonded and 1400 cm^{-1} if free. We see in conformers 1, 2, and 4 the deformation modes occur near 1380 cm^{-1}, while in conformer 2, one of the deformation modes is indeed 1423 cm^{-1}, confirming its role in the hydrogen bonding to the water. The CH_3 symmetrical bend has an experimental frequency of 1400 cm^{-1}. We conclude that the frequency differences for characteristic modes on different isomers are large enough to be experimentally observed (10−50 cm^{-1}) and in some cases are indicative of hydrogen-binding environments.

E. Tunneling Effects. It has been suggested from calorimetric studies that proteins exhibit quantum tunneling effects.[49,50] However, these measurements are of a macroscopic nature, and identification of the specific motions involved in tunneling for proteins was not carried out. We report here tunneling calculations with full assignment of the motions involved. A key issue is, of course, to establish weather the tunneling splittings are large enough to be spectroscopically observable. For the peptide di-L-serine, we have identified two possible tunneling motions: the methyl librational about the

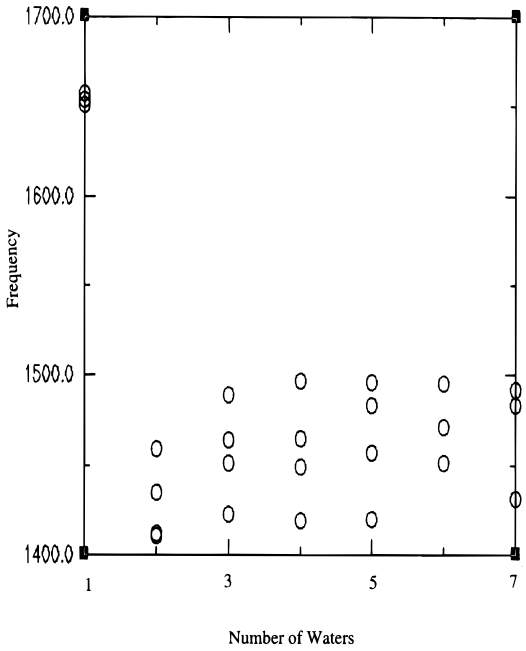

Figure 8. CH_3 asymmetric bending mode as a function of additional H_2O added to the peptide. The frequencies are in cm^{-1}.

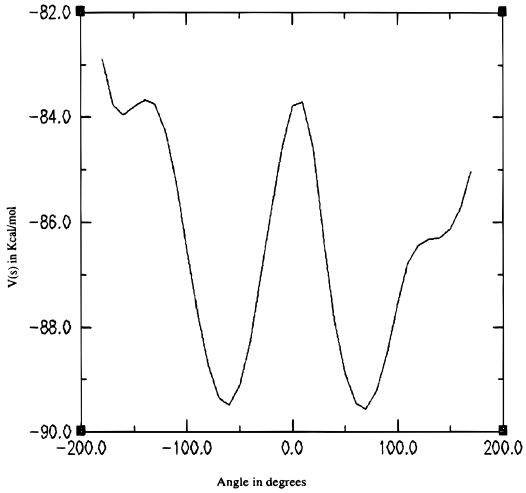

Figure 9. H_2O flipping motion $V(s)$ along tunneling path s. The angle is the angle of the serine OH to the plane of the water.

carboxy and nitro terminus, and the H_2O flipping against the peptide. For motion corresponding to these two tunneling states, we calculated the potential along the tunneling path, s, by an adiabatical mapping method. For the methyl rotations, the adiabatic coordinate corresponds to the torsion angle (H−C−C−O and H−C−N−H), and for H_2O flipping motion the adiabatic coordinate is the angle between the serine O−H and the H_2O. The tunneling probability and hence tunnel splitting were calculated by assuming a monodimensional symmetrical potential, $V(s)$, and using the WKB (Wentzel, Kramers, and Brillouin) approximation.[51] Within the WKB approximation the tunneling rate is given by

$$\nu_t = \frac{\omega}{\pi}\exp(-\theta) \tag{4.1}$$

where

$$\theta = \frac{1}{\hbar}\int [2\mu(V(s) - E)]^{1/2}\,ds \tag{4.2}$$

In eq 4.3, for the methyl tunneling, μ is replaced with I, the

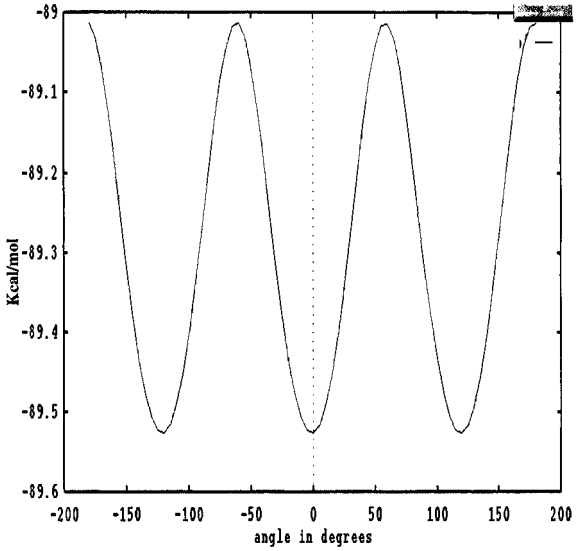

Figure 10. Methyl potential $V(s)$ along tunneling path s for the carboxyl end of the peptide.

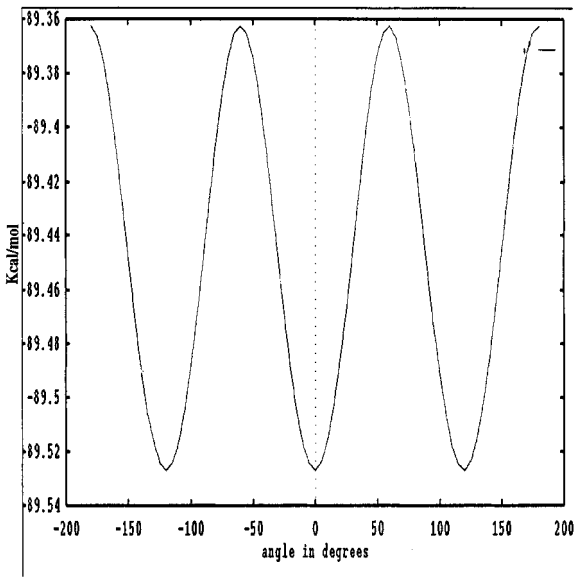

Figure 11. Methyl potential $V(s)$ along tunneling path s for the nitro end of the peptide.

moment of inertia of the methyl, and ω is the librational frequency. Figures 10 and 11 illustrate the tunneling potential for the carboxy and nitro terminal methyl groups, respectively (for conformer 1). The double-well tunneling potential for the H_2O flipping motion is shown in Figure 9. For this motion we found a barrier height of 4.4 kcal/mol (conformer 1) and hence a tunneling frequency of roughly 160 MHz. Our calculated barrier for the H_2O flipping motion in the peptide system is higher than for small $(H_2O)_n$ clusters, which have barriers between 0.2 and 2.2 kcal/mol.[52,53] One reason our barrier is higher than for the water clusters is because conformer 1 has three hydrogen bonds between the H_2O and peptide which must be broken when flipped.

The barrier height, measured from the zero-point energy, for the carboxy terminal methyl group is 0.281 kcal/mol (98.35 cm^{-1}), and thus the librational frequency calculated by solving the one-dimensional Hamiltonian is 22 cm^{-1}. From eqs 4.2 and 4.3, the tunnel splitting for this methyl group is 30.27 GHz (1.01 cm^{-1}). The story for the nitro terminal methyl group is quite different. The barrier height in this case is only 0.063 kcal/mol (22.05 cm^{-1}), which is lower than the first librational

excited state at 27.45 cm^{-1}. Thus our calculated tunneling probabilities and frequencies are high at 58.46 GHz (1.95 cm^{-1}). Although our frequencies for the methyl libration are reasonable and compare well with those of dimethyl-*s*-tetrazine in durene crystals (15−20 cm^{-1}),[54] our barrier heights and hence tunneling frequencies are quite different and are more like a nearly free methyl rotator. The barrier of methyl tunneling is quite sensitive to the electronegativity of the adjacent atoms; thus, even a slight error in the atomic partial charge may cause larger errors in the barrier heights. Because the neutral blocked peptide is not a naturally occurring structure, the parameters for these terminal methyl groups were fitted from a calculation to the barrier height for ethane. The barrier height is obviously in question; however, the results suggest that tunnel splittings associated with the CH_3 rotations in the peptide may be measured directly in high-resolution frequency-domain spectroscopy. The same is not true for the H_2O flipping motions mentioned above. Perhaps a possible approach for these motions will be to use time-domain techniques as the tunneling time is long.

V. Results: Trialanine in Antiparallel (AP) β Pleated Sheet Configuration

In a previous section we found that the calculated vibrational frequencies are strongly dependent on the force field used. This section of the paper will provide a test of the Amber force field against existing experimental frequencies. For this comparison, we choose to look at trialanine in a β sheet configuration. This structure has well-defined experimental and empirically derived frequencies. Trialanine (Ala_3) is known to crystallize in both parallel (P)[55] and antiparallel (AP)[56] β sheet configuration and is an inhibitor of the esterolytic activity of elastace.[57] The structure and IR, Raman spectrum of Ala_3 for both configurations is given by Qian et al.[12]

Qian and co-workers also derived a harmonic empirical force field for this system as a least-squares fit to experimental IR and Raman data for β -poly(L-alanine).[58] The force field is then further refined for Ala_3 in the CO_2^- wagging coordinate, the C═O stretch, and the hydrogen-bonded H···O coordinate in order to include some anharmonic effects due to hydrogen bonding.[2] Table 4 lists the calculated frequencies for both the all-atom force field using the VSCF method as in the peptide calculations and the experimental frequencies (IR, Raman) and the frequencies from the empirical force field of Qian et al. (empirical).

In Table 4 many of the frequencies are listed as doublets, which belong to either the A or B sheet of the Ala_3 configuration. For the empirical frequencies, the doublets usually appear as degenerate pairs due to symmetry considerations, as in a harmonic oscillator approximation they are nearly identical. However in the VSCF calculation these splittings will become quite pronounced, particularly in the low-frequency region, where we observe splitting up to 10 cm^{-1}. In the discussion below we will consider each region of the spectrum separately and group these modes based their characteristic features. The modes were assigned by an analysis of the corresponding eigenvectors from the diagonalization of the Hessian matrix.

Amide I (1690−1620 cm^{-1}). The higher frequency amide I modes (1691−1667 cm^{-1}) in the empirical spectrum do not occur in degenerate pairs because these frequencies were calculated by the dipole derivative coupling (DDC) method by Qian and co-workers.[59] In the VSCF spectrum the high-frequency and relatively low intensity modes (1706−1702 cm^{-1}) are higher than the empirical and the experimental frequencies, indicating a significant weakness of the current all-atom force field. The most intense experimental IR and Raman band occurs between 1647 and 1641 cm^{-1} (IR) and at 1658 cm^{-1} (Raman), which are the main amide I modes. For β sheet structures, the characteristic amide I modes generally show a strong adsorption at 1632 cm^{-1} and a weaker adsorption at 1690 cm^{-1}, but this can depend on intersheet hydrogen bonding.[14] Previous predictions by Bandekar and Krimm suggested that the amide I frequencies for an infinite parallel chain β sheet poly-L-alanine occur at 1663 and 1642 cm^{-1}.[59] For these intense modes we are in good agreement with both the experimental frequencies and the frequencies from the fitted force field.

Amide II (1580−1520 cm^{-1}). The amide II region, characteristic of an NH in-plane bend, has very intense IR bands at 1547 and 1536 cm^{-1}. Again for these bands, Qian and co-workers used the DDC dipole derivative coupling method to calculate the shifted empirical frequencies, which are 1558 and 1531 cm^{-1}. Our present VSCF calculation predicts the amide II frequencies to be at 1554 and 1531 cm^{-1}, in good agreement with the experiments. The weaker Raman band at 1536 cm^{-1} is difficult to assign. Qian places this band at 1533 cm^{-1}; however, our calculations suggest it lies at 1542 cm^{-1}. Furthermore, our present calculation predicts two additional doublets at 1500 cm^{-1}, which would be part of the experimental IR shoulder at 1508 cm^{-1}. The Amber force field seems to agree better with the experimental data than the harmonic force field for these frequencies.

CH_3 Modes (1450−1380 cm^{-1}). In organic molecules and proteins, the characteristic methyl asymmetric bend occurs at 1460 cm^{-1}.[60,61] Our present calculation is in excellent agreement with this predication. There is a striking feature in the VSCF spectrum at 1420 cm^{-1}. Generally, there are two groups that absorb here: a shoulder peak at 1422 cm^{-1} for the methyl asymmetric stretch, and a CN stretch for the amide III modes (1420−1405 cm^{-1}).[60] While we predict the amide III CN stretch to lie at 1412 cm^{-1}, we also suggest that a shoulder peak around 1422 cm^{-1} should be seen experimentally. Curiously this is absent in both the experimental and empirical frequencies for the antiparallel configuration; however, for the parallel configuration there is a shoulder at 1421 cm^{-1} in the experimental IR spectrum.[21] The empirical calculation does not seem to be able to reproduce this shoulder peak for either configuration and is inconclusive on the amide III CN stretch. The VSCF symmetric methyl bending modes are in good agreement with both the empirical and experimental frequencies (1364 cm^{-1}).

Amide III (1350−1200 cm^{-1}). The amide III mode is characteristic of an NH in-plane bend plus a CN stretch; however, the frequencies will also depend on the backbone conformation and residue composition. The observed frequencies show a very weak band at 1353, with stronger bands at 1268 and 1234 cm^{-1}. The spectrum is complicated by the NH_3^+ rocking modes at 1330 and 1323 cm^{-1}. While our predicted frequencies match well with the more intense bands of the amide III modes, we are unable to predict the very weak mode at 1353 cm^{-1}, again indicating that our present force field could use refinement in the description of the amide bond.

Skeletal Modes (1200−850 cm^{-1}). From about 1200−850 cm^{-1} is where most of the NC, CC stretch, and CH stretch−bend frequencies occur and is also where the anharmonic and mode-coupling effects become more dramatic. In general, all of our methyl combination stretch−bend and rocking frequencies (1158, 1148, and 1122 cm^{-1}) are lower than the experimental frequencies by 20 cm^{-1}. However, the empirically fitted frequencies are also in error by 15 cm^{-1}, indicating that the anharmonic and mode-coupling effects are important in this region. One reason that the all-atom force field is in error in

TABLE 4: Experimental and Calculated Frequencies (in cm^{-1} for $Ala_3(Ap)$)[a]

experimental		calculated			experimental		calculated		
Raman	IR	empirical	VSCF	assignment	Raman	IR	empirical	VSCF	assignment
	1691(MW)	1686	1706	amide I			1083, 1083	1093, 1090	CH_3(r), CC(s)
		1681	1706	amide I	1082(S)	1083(VW)	1083, 1083	1089, 1088	CH_3(r), CC(s)
	1667(sh)	1666	1704	amide I	1077(sh)	1077(sh)	1066, 1066	1087, 1085	CH_3(r), CC(s)
1667(sh)		1665	1702	amide I	1067(VW)		1064, 1064	1076, 1058	CH_3(r)
1658(S)		1657	1656	amide I			1064, 1064	1055, 1054	CH_3(r)
1639(sh)	1647(sh)	1645, 1645	1647, 1644	amide I	1054(MW)	1055(MS)	1063, 1063	1046, 1046	CH_3(r)
	1641(VS)	1643	1631	amide I			1061, 1061	1041, 1039	CH_3(r), CC(s)
		1636, 1636	1630, 1629	amide I		1050(sh)	1059, 1059	1033, 1032	CH_3(r), CC(s)
	1623(W)	1630, 1630	1625, 1624	amide I			1051, 1051	1029, 1028	CH_3(r), CC(s), NH_3^+(r)
		1608, 1608	1623, 1624	amide I	1018(W)	1016(M)	1046, 1046	1015, 1013	CH_3(r), CC(s), NH_3^+(r)
	1613(VW)	1607, 1607	1618, 1612	amide I		967(S)	964, 964	971, 972	CH_3(r), CN(s)
	1595(W)	1597, 1597	1596, 1595	CO_2^-(as)	960(MW)	961(sh)	963, 963	984, 949	CH_3(r), CN(s)
		1596, 1596	1591, 1587	CO_2^-(as)	944(VW)	949(W)	944, 944	944, 944	CH_3(r), CN(s)
		1571	1587	amide II			942, 942		NC(s)
		1567, 1567	1575, 1566	amide II	920(sh)	924(sh)	923, 923	927, 921	NC(s)
	1547(S)	1558	1554	amide II		918(sh)	919, 919	922, 913	NC(s)
1551(W)		1557	1553	amide II			905, 905	896, 892	CN(s)
1536(W)			1544, 1541	amide II	902(VS)	900(MW)	900, 900	892, 880	CN(s)
		1533	1532	amide II		882(W)	880, 880	877, 868	CC(s), CO(b)
	1536(S)	1531, 1531	1531, 1524	amide II	876(VW)	875(VW)	876, 876	866, 865	CC(s), CO_2^-(sb)
		1517, 1517	1520, 1520	amide II	861(MW)	861(MW)	847, 847	865, 863	CC(s), CO_2^-(sb)
	1508(sh)	1515, 1515	1513, 1511	amide II		848(W)	844, 844	854, 849	NC(s), CC(S)
			1505, 1498	amide II				843, 841	NC(s), CC(S)
			1494, 1491	amide II				831, 831	NC(s), CC(S)
		1455, 1455	1487, 1471	CH_3(ab)				803, 800	NC(s), CC(s)
1471(sh)		1455, 1455	1470, 1468	CH_3(ab)	789(VW)	790(W)	778, 778	803, 800	CO(opb)
1457(MS)	1459(MS)	1453, 1453	1465, 1460	CH_3(ab)		774(MW)	774, 774	778, 777	CO(opb)
	1447(W)	1453, 1453	1453, 1449	CH_3(ab)	769(sh)		766, 766	763, 756	CO(opb), CO_2^-(w,b)
	1443(VW)	1452, 1452	1444, 1442	CH_3(ab)	760(W)	761(sh)	759, 759	754, 745	CO(opb), CO_2^-(w,b)
		1452, 1452	1443, 1442	CH_3(ab)	725(W)	725(W)	725, 725		amide V
		1452, 1452	1438, 1437	CH_3(ab)			714, 714	710, 708	CN(t), CO_2^-(w)
		1452, 1452	1437, 1435	CH_3(ab)			703, 703	705, 701	CC(s), CN(t), NH(opb)
		1452, 1452	1436, 1434	CH_3(ab)	695(VW)	696(VS)	692, 692	686, 678	CN(t), amide V
		1452, 1452	1430, 1429	CH_3(ab)		687(W)	690, 690	670, 662	CN(t), amide V
		1451, 1451	1433, 1431	CH_3(ab)	677(W)	675(VW)	683, 683	639, 627	CN(t), amide V
		1451, 1451	1431, 1429	CH_3(ab)	654(VW)	655(MS)	661, 660	620, 613	CO_2^+(b), CO(ipb),CC(s), amide V
			1429, 1427	CH_3(ab)			637, 637	610, 603	CO(ipb)
			1425, 1425	CH_3(ab)	633(W)	632(MS)	633, 633	602, 599	CO(ipb)
			1424, 1424	CH_3(ab)	592(VW)	593(W)	577, 577	596, 592	NCC(d), CO_2^-(r)
			1422, 1422	CH_3(ab)			570, 570	588, 571	CO_2^-(r)
			1421, 1421	CH_3(ab)			532, 531	569, 566	CN(t), NH(t)
			1420, 1420	CH_3(ab)			518, 517	523, 520	hydrogen bond(s)
			1420	CH_3(ab)			516, 517		hydrogen bond(s)
		1411, 1411		CO_2^-(s,ab), CC(b)			510, 510	509, 502	CN(t)
1409(MW)	1411(S)	1410, 1410	1415, 1412	CO_2^-(s,ab), CC(s), amide III	489(VW)	490(VW)	489, 489	488, 481	NCC(d), hydrogen bond(s), CC(b), NH(opb)
		1402, 1402		CH_3(sb), NH(ipb)	458(W)	462(MS)	454, 454	478, 464	CC(b)
1396(W)	1400(sh)	1400, 1400	1406, 1404	CH_3(sb), NH(ipb)			451, 451	458, 452	CC(b)
		1388, 1388		CH_3(sb)				449, 446	CC(b), NH(opb)
		1387, 1387		CH_3(sb)	436(MW)		421, 421	431, 425	CC(b), NH(opb)

1379(W)	1377(MW)	1382, 1382	1373, 1370	CH_3(sb)	396(VW)		413, 413	407, 405	CC(b), NH(opb)
		1382, 1382		CH_3(sb)				416, 393	CC(b), NH(opb)
1363(MW)	1364(MS)	1373, 1371	1365, 1358	CH_3(sb)				387, 378	CC(b), NH(opb)
		1372, 1372		CH_3(sb)			353, 352	362, 358	CO_2^-(r), CC(b)
1353(VW)	1352(VW)	1350, 1350		amide III	345(VW)		349, 348	347, 341	CC(b), CCN(d), CO_2^-(r)
		1348, 1348		amide III	325(VW)		318, 318	339, 323	CC(b), CO_2^-(w), CO(ipb)
1330(sh)	1331(W)	1322, 1322	1328	NH_3^+(ab), NH_3^+(r)	306(MW)		303, 303	311, 304	NCC(d), CO_2^-(w), CC(b)
1323(W)	1323(W)	1315, 1315	1315, 1314	NH_3^+(ab), NH_3^+(r)			300, 299	298, 297	CC(b), NCC(d), CO(ipb)
1307(MW)	1306(W)	1308, 1308	1307, 1281	H(b,r)	293(sh)		296, 294	291, 291	CC(b), NCC(d), CO(ipb)
		1296, 1296		NH_3^+(ab), NH_3^+(r)				394, 316	CC(t)
1266(MS)	1268(M)	1270, 1270	1268, 1257	amide III				370, 366	CC(t)
		1264, 1264		amide III				313, 310	CC(t)
1247(MW)	1248(sh)	1263, 1263	1247, 1244	amide III				307, 297	CC(t)
		1263, 1263		amide III				291, 285	CC(t)
	1242(sh)	1258, 1258	1240, 1235	amide III			290, 290	289, 289	CC(b), NCC(d), CO(ipb)
1229(MS)	1234(MS)	1234, 1234	1233, 1230	amide III			285, 285	288, 291	CC(b), NCC(d), CO(ipb)
	1221(VW)	1210, 1210	1222, 1221	NC(s), CC(s)			265, 264	281, 279	CO_2^-(r), CC(t)
	1206(VW)	1207, 1207	1221, 1200	NC(s), CC(s)	269(VW)		255, 255	272, 272	CC(t), CC(b)
		1196, 1196	1195, 1193	NC(s), amide III	251(sh)	251, 250	270, 267	CC(t)	
		1193, 1193	1191, 1190	NC(s), amide III	242(M)	249	254, 242	CC(t)	
1169(sh)		1179, 1179	1163, 1161	NC(s), CC(s), NH_3^+ (r)			241, 241		CC(t)
		1176, 1176	1139, 1137	NC(s), CC(s), NH (ipb)			241, 241		CC(t)
1159(MW)	1158(MW)	1171, 1171	1134, 1134	CH_3(sb,r)			236, 236		CC(t)
		1170, 1170	1127, 1121	CH_3(sb,r)			233, 233		CC(t), CO_2^-(r)
1146(sh)	1148(MS)	1139, 1139	1123, 1116	CH_3(sb,r)	226(VW)		229, 229	213, 216	CC(t), CO_2^-(r)
		1137, 1137	1112, 1112	CH_3(sb,r)			224		CC(b)
1120(VW)	1122(W)	1124, 1124	1109, 1106	CH_3(sb,r)			223		CO_2^-(r)
1108(MW)	1110(W)	1120, 1120	1102,1101	CH_3(sb,r)			222		CC(t), CCN(d)
		1089, 1089	1098, 1095	CH_3(r), CC(s)			221		CC(b)
	1090(VW)	1087, 1087	1095, 1093	CH_3(r), CC(s)			213, 215	207, 196	CC(b)

[a] as = asymmetric stretch, ss = symmetric stretch, b = bend, ipb = in-plane bend, opb = out-of-plane bend, t = torsion, d = distortion, r = rocking, w = wagging, S = strong, M = medium, W = weak, V = very, sh = shoulder.

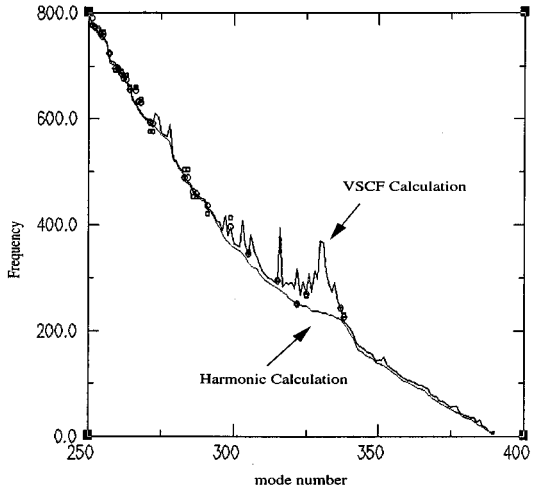

Figure 12. Harmonic and corresponding VSCF frequencies for ALA_3 in AP β sheet configuration. The circles correspond to the empirical frequencies, and the squares are the experimental frequencies. Below 200 cm^{-1} the empirical and experimental data were not available. The mode number is the enumeration of the mode position (from highest to lowest frequency). The frequencies are in cm^{-1}.

this region may be that it was derived for smaller organic molecules, which have methyl rocking modes between 1141 and 1132 cm^{-1}.[60] The VSCF frequencies for this mode lie between 1134 and 1106 cm^{-1}. We are however, in better agreement with the backbone NC and CC stretching frequencies and in some cases surpass the empirically fitted frequencies, which can be in error by 30 cm^{-1} (1016 cm^{-1}).

Amide V (725−675 cm^{-1}). The amide V modes are characterized by the NH out-of-plane bend plus a CN torsion and is marked by a very intense band near 700 cm^{-1}. Both the current force field and the empirical frequencies correctly predict this mode; however, for the very weak frequency at 675 cm^{-1} our VSCF frequencies are much too low (635 cm^{-1}).

Low-Frequency Regime (600−200 cm^{-1}). The low-frequency region is quite difficult to assign and must be considered suggestive at best. Frequencies below 200 cm^{-1} were not assigned in the experimental or empirical spectrum. The VSCF calculated CO_2^- rocking mode at 593 cm^{-1} is in excellent agreement with the experimental frequency, as are many of the low frequencies. It is in this region where the VSCF frequencies usually surpass the empirically fitted frequencies, as our calculation includes the anharmonic and mode-coupling effects which are so important here. In this region we also begin to see further manifestations of the highly anharmonic methyl rotational (CC(t)) modes (Figure 12). In Figure 12 we plot the harmonic frequencies and overlapping on these the VSCF frequencies as a function of mode number. A comparison is also made with the empirical (circles) and experimental (squares) frequencies of Qian and co-workers, based on their normal mode assignment. It is quite clear that in this region the harmonic approximation breaks down rather severely. This is in part why the empirically fitted frequencies, which rely on harmonic fitted force constants, begin to deviate from the experimental spectrum. In the VSCF calculation we see that some of the methyl torsion modes that occur between 394 and 285 cm^{-1} have much lower counterparts in the empirical spectrum (241−233 cm^{-1}). Because the assignment of the experimental frequencies is inconclusive, it is hard to say where exactly the experimental torsional modes should lie.

As a global measure for the quality of reproducing the experimental frequencies, we calculate the rms deviation between the calculated and experimental frequencies, for lines of medium intensity and higher. The rms deviation for the empirical frequencies is 8.4 cm^{-1}, while the VSCF deviation is higher at 12.61 cm^{-1}. The listed set of measured frequencies is rather incomplete, and also we do not calculate the absolute intensities as a further comparisons. Therefore the present study offers only a very limited test of the Amber force field. Nevertheless, we do find overall discrepancies in frequencies between the Amber force field and the experimental data for the low-intensity amide modes (1690, 1353, and 675 cm^{-1}) as well as the CH_3 (sb,r) modes (1159−1108 cm^{-1}). These discrepancies are sufficient to demonstrate that at least a partial revision of this widely used force field is justified.

VI. Conclusions

In this paper we begin to address the issue of conformational analysis of proteins using vibrational spectroscopy. We began with the anstaz that for many of the modes in condensed systems, e.g. proteins, we can use the near-separability of the normal mode degrees of freedom to reduce the fully *N*-dimensional coupled Hamiltonian into *N* single-mode equations (eq 3.3). We further restrict the coupling between the modes to occur in a pairwise manner, such that a quartic expansion of the potential is realized (eq 3.6). We illustrated that for many modes of the system this approximation is valid; however, for the methyl torsional modes the expansion breaks down (Figure 1). Using the VSCF method we first address the issue of the solvent force field. We compare the MOIL version of the water potential that includes intermolecular motion of H_2O with the force field utilized in the earlier work of Coker and Watts. We see that in addition to changes in the water vibrational spectrum (symmetric stretch and bend) a few of the peptide−H_2O coupled modes are also shifted by as much as 50 cm^{-1}. This indicates that the solvent force field will play a relatively important role in protein spectroscopy. We also compare the harmonic frequencies to the full VSCF frequencies and see that for many modes the harmonic representation is quite poor. This is born out in particular for the water sheering motion against the peptide and the methyl rotations, as well as the hydrogen-bonding description of the water−peptide complex. This suggests that any complete calculation of condensed-phase spectroscopy should adequately account for these effects.

We further identified *six* new H_2O−peptide modes, which reflect the environment of the water in the hydrogen-binding pocket of the peptide. We can identify the nature of the hydrogen binding as seen through the shifts in characteristic frequencies of the water symmetric stretch, the peptide amide I bands, and the OH deformation modes. These findings should be an advantage to the experimentalist in determining conformer geometry. We do note, however, that refinement of the current force field is imperative, as some of the modes do not fall within their expected range. We have also investigated the possibility of tunneling within our peptide system. We find that for conformer 1 the tunneling frequencies of the water flipping motion is small; however, the methyl tunneling frequencies are unusually high (1.01 and 1.95 cm^{-1}). Because our barriers suggest a rather free rotor, we are under the impression that an inaccuracy in the electrostatic potential exists for these end groups.

Last we address the issue of real spectroscopy for larger systems, namely trialanine in antiparallel β sheet configuration. We compare our VSCF frequencies with the experimental and empirical frequencies of Qian and co-workers.[12] We find that with respect to the intense lines in the spectrum, we are in general agreement with the experimental and empirically fitted frequencies. However, a few low-intensity lines can differ quite

strongly, indicating a real need for refinement of the current force field. More demanding tests which include absolute intensities are clearly desirable as the basis for future potential refinement applications.

Acknowledgment. This work was supported by grants from the Israel Ministry of Science (R.B.G.) and from the National Institutes of Health (GM41905) (R.E.). The calculations were carried out on the SP2 parallel computer system of the Israel Inter-University Computing Center. We thank Dr. Y. Kimhi for his help in using the SP2 system, and Dr. Roitberg for careful reading of the manuscript. S.K.G. extends many thanks to the Hebrew University for a Lady Davis Fellowship. Involved in many ways in this work are the suggestions and bright ideas of Joon Jung and Masha Niv.

References and Notes

(1) McCammon, J. A.; Harvey, S. C. *Dynamics of Proteins and Nucleic Acids*; Cambridge Unviersity Press: Cambridge, 1987.
(2) Cornell, W. D.; Cieplak, P.; Bayly, C. I.; Gould, I. R.; Merz, K. M., Jr.; Ferguson, D. M.; Spellmeyer, D. C.; Fox, T.; Caldwell, J. W.; Kollman, P. A. *J. Am. Chem. Soc.* **1995**, *117*, 5179.
(3) Jorgensen, W. L.; Tirado-Rievs, J. *J. Am. Chem. Soc.* **1988**, *110*, 1657.
(4) Brooks, B. R.; Bruccoleri, R. E. Olafson, B. D.; States, D. J.; Swaminathan, S.; Karplus, M. *J. Comput. Chem.* **1983**, *4*, 187.
(5) Lakhlifi, A.; Picaud, S.; Girardet, C.; Allouche, A. *Chem. Phys.* **1995**, *201*, 73.
(6) Jansen, G. *J. Chem. Phys.* **1996**, *105*, 89.
(7) Moulin, V.; Schriver, A.; Achriver-Mazzouli, L.; Chaquin, P. *Chem. Phys. Lett.* **1996**, *263*, 423.
(8) Tosa, V.; Isomura, S.; Kuga, Y.; Takeuchi, K. *Vibrat. Spectrosc.* **1994**, *8*, 45.
(9) Xie, Y. M.; Davy, R. D.; Yates, B. F.; Blahous, C. P. *Chem. Phys.* **1989**, *135*, 179.
(10) Lim, M.; Jackson, T.; Anfinrud, P. *J. Chem. Phys.* **1995**, *102*, 4355.
(11) Krimm, S.; Reisdorf, W. C. *Faraday Discuss. Chem. Soc.* **1994**, *99*, 181.
(12) Qian, W.; Bandekar, J.; Krimm, S. *Biopolymers* **1991**, *31*, 193.
(13) Haris, P. I.; Chapman, D. *Biopolymers* **1995**, *37*, 251.
(14) Susi, H.; Timasheff, S. N.; Stevens, L. *J. Biol. Chem.* **1967**, *242*, 5460.
(15) Swivedi, A. M.; Krimm, S. *Macromolecules* **1982**, *15*, 186.
(16) Cherepy, N. J.; Shreve, A. P.; Moore, L. J.; Franzen, S.; Boxer, S. G.; Mathies, R. A. *J. Phys. Chem.* **1994**, *98*, 6023.
(17) Myers, A. B. *Chem. Phys.* **1994**, *180*, 215.
(18) Cusack, S.; Smith, J.; Finney, L. J.; Tidor, B.; Karplus, M. *J. Mol. Biol.* **1988**, *202*, 903.
(19) Smith, J.; Tidor, B.; Karplus, M. *J. Chem. Phys.* **1990**, *93*, 2974.
(20) Martinez, S. J., III; Alfano, J. C.; Levy, D. H. *J. Mol. Spectrosc.* **1993**, *158*, 82.
(21) Martinez, S. J., III; Alfano, J. C.; Levy, D. H. *J. Mol. Spectrosc.* **1991**, *145*, 100.
(22) Ermer, O.; Lifson, S. *J. Am. Chem. Soc.* **1973**, *95*, 4121.
(23) Allinger, N. *J. Am. Chem. Soc.* **1977**, *99*, 8127.
(24) Warshel, A.; Levit, M.; Lifson, S. *J. Mol. Spectrosc.* **1970**, *33*, 84.
(25) Momany, F.; McGuire, R.; Burgess, A.; Scherage, H. *J. Phys. Chem.* **1975**, *79*, 2361.
(26) Bowman, J. M. *J. Chem. Phys.* **1978**, *68*, 608.
(27) Gerber, R. B.; Ratner, M. A. *Chem. Phys. Lett.* **1979**, *68*, 195.
(28) Bowman, J. M. *Acc. Chem. Res.* **1986**, *19*, 202.
(29) Jung, J. O.; Gerber, R. B. *J. Chem. Phys.* **1996**, *105*, 10682.
(30) Jelski, D. A.; Haley, R. H.; Bowman, J. M. *J. Comput. Chem.* **1996**, *17*, 1645.
(31) Jung, J. O.; Gerber, R. B. *J. Chem. Phys.* **1996**, *105*, 10332.
(32) Roitberg, A.; Gerber, R. B.; Elber, R.; Ratner, M. A. *Science* **1995**, *268*, 1319.
(33) Dunbrack, R. L.; Karplus, M. *Nat. Struct. Biol.* **1994**, *1*, 334.
(34) Levy, R. M.; Karplus, M.; Kurshick, J.; Perahia, D. *Macromolecules* **1984**, *17*, 1370.
(35) Levy, R. M.; Karplus, M.; Perahia, D. *Proc. Natl. Acad. Sci.* **1982**, *79*, 1346.
(36) Go, N.; Noguti, T.; Nishikawa, T. *Proc. Natl. Acad. Sci.* **1983**, *80*, 3696.
(37) Elber, R.; Roitberg, A.; Simmerling, C.; Goldstein, R.; Li, H.; Verkhivker, G.; Keaser, C.; Zhang, J.; Ulitsky, A. *Comput. Phys. Commun.* **1994**, *91*, 159.
(38) Coker, D. F.; Watts, R. O. *J. Phys. Chem.* **1987**, *91*, 2513.
(39) Reimers, J. R.; Watts, R. O.; Klein, M. L. *Chem. Phys.* **1982**, *64*, 95.
(40) Gerber, R. B.; Ratner, M. A. *Adv. Chem. Phys.* **1988**, *70*, 97.
(41) Nielsen, H. H. *Rev. Mod. Phys.* **1951**, *23*, 90.
(42) Schneider, W.; Thiel, W. *Chem. Phys. Lett.* **1989**, *157*, 367.
(43) Yang, W.; Peet, A. C. *Chem. Phys. Lett.* **1988**, *153*, 98.
(44) Ulitsky, A.; Elber, R. *J. Chem. Phys.* **1993**, *98*, 3380.
(45) Roitberg, A.; Elber, R. *J. Chem. Phys.* **1991**, *95*, 9227.
(46) Chen, X. G.; Schweitzer-Stenner, R.; Krimm, S.; Mirkin, N. G.; Asher, S. A. *J. Am. Chem. Soc.* **1994**, *116* 11141.
(47) Alpert, N. L.; Keiser, W. E.; Szymanski, H. A. *IR: Theory and Practice of Infrared Spectroscopy*; Plenum Pub. Corp.: New York, 1970.
(48) Pribble, R. N.; Zwier, T. S. *Science* **1994**, *265*, 75.
(49) Bell, R. P. *The Tunnel Effect in Chemistry*; Chapman and Hall: New York, 1980.
(50) Franke, M.; Winkler, H.; Trautwein, A. X.; Parak, F. *Hyperfine Interact.* **1992**, *71*, 1291.
(51) Pauling, L.; Bright Wilson, E. *Introduction to Quantum Mechanics*; McGrw-Hill Book Co., Inc.: New York, 1935.
(52) Liu, K.; Saykally, R. J. *Science* **1996**, *271*, 929.
(53) Liu, K.; Brown, M. G.; Cruzan, J. D.; Saykally, R. J. *Science* **1996**, *271*, 62.
(54) Hartmann, M.; Miller, R. E.; Toenies, J. P.; Vilesov, A. F. *Science* **1996**, *272*, 1631.
(55) Hempel, A.; Camerman, N.; Camerman, A. *Biopolymers* **1991**, *31*, 192.
(56) Fawcett, J. K.; Camerman, N.; Camerman, A. *Acta Crystallogr. B* **1975**, *31*, 658.
(57) Dzialoszynski, L.; Hofmann, T. *Biochim. Biophys. Acta* **1973**, *302*, 406.
(58) Rabolt, J. F.; Moore, W. H.; Krimm, S. *Macromolecules* **1977**, *10*, 1065.
(59) Bandekar, J.; Krimm, S. *Biopolymers* **1988**, *27*, 885.
(60) Conley, R. T. *Infrared Spectroscopy*; Allyn and Bacon, Inc.: New York, 1972.
(61) Hester, R. E.; Girling, R. B. *Spectroscopy of Biological Molecules*; The Royal Society of Chemistry: Letchworth, U.K., 1991.